Published in final edited form as:
Nat Mater. 2013 June ; 12(6): 576–583. doi:10.1038/nmat3627.

Nano-analytical electron microscopy reveals fundamental insights into human cardiovascular tissue calcification

Sergio Bertazzo[1,2], **Eileen Gentleman**[1,2,5], **Kristy L. Cloyd**[1,2], **Arian H. Chester**[4], **Magdi H. Yacoub**[4], and **Molly M. Stevens**[1,2,3,*]

[1]Department of Materials, Imperial College London, London SW7 2AZ, UK

[2]Institute of Biomedical Engineering, Imperial College London, London SW7 2AZ, UK

[3]Department of Bioengineering, Imperial College London, London SW7 2AZ, UK

[4]National Heart & Lung Institute, Harefield Heart Science Centre, Imperial College London, Harefield, Middlesex UB9 6JH, UK

[5]Department of Craniofacial Development and Stem Cell Biology, King's College London, London SE1 9RT, UK

Abstract

The accumulation of calcified material in cardiovascular tissue is thought to involve cytochemical, extracellular matrix and systemic signals, however, its precise composition and nano-scale architecture remain largely unexplored. Using nano-analytical electron microscopy techniques, we examined valves, aortas, and coronary arteries from patients with and without calcific cardiovascular disease and detected spherical calcium phosphate particles, regardless of the presence of calcific lesions. While tissue marked by calcific lesions immunogold labelled for the bone-specific protein osteocalcin, tissue on which particles alone were present only expressed early osteoblastic transcription factors, suggesting that the localization of spherical particles may precede the appearance of mature osteoblasts and calcific lesions. We also examined lesions after sectioning with a focused ion beam and found that spherical particles are composed of highly crystalline hydroxyapatite which crystallographically and structurally differed from bone mineral. Taken together, these data suggest that mineralized spherical particles may play a fundamental role in calcific lesion formation. Their ubiquitous presence in varied cardiovascular tissues and from patients with a spectrum of diseases, further suggests that lesion formation may follow a common process. Indeed, applying materials science techniques to ectopic and orthotopic calcification has great potential to lend critical insights into pathophysiological processes underlying calcific cardiovascular disease.

[*]To whom all correspondence should be addressed.

Financial Disclosure
The authors declare no competing financial interests.

Author Contributions
S.B. designed the study, performed sample preparation, conducted all the experimental work, carried out data interpretation and aided with manuscript preparation and writing. E.G. aided with study design and data interpretation and wrote the majority of the manuscript. K.L.C. helped with sample preparation. A.H.C. and M.H.Y helped with sample procurement and aided in data interpretation. M.M.S. supervised the study, aided with study design, data interpretation and revised the manuscript.

Europe PMC Funders Author Manuscripts

Calcification in the cardiovascular system is a widespread phenomenon involved in several diseases that taken together contribute to 17 million deaths per year1. Calcific aortic valve disease (CAVD) is present in 26% of the population over the age of 65 and up to 50% of those over 852,3, and remains the most common cause of valve stenosis, which can lead to heart failure4,5. Calcific lesions can also be found in the mitral valve, often resulting from rheumatic fever (which remains prevalent in children in developing countries6), and in coronary and other arteries. Indeed, atherosclerotic plaques containing calcific lesions are reported in more than 65% of the population over the age of 407. Currently there is no treatment to reverse cardiovascular calcification associated with arteriosclerosis8, but incompetent calcified valves can be surgically replaced with mechanical or bioprosthetic implants. Valve replacement procedures account for 22% of all cardiac surgeries, and among these AV procedures are by far the most common6. Such surgeries, however, carry an operative mortality in the range of 3%9,10 and only alleviate symptoms of the end-stage disease.

Calcific lesions are thought to form from cardiovascular cells (such as vascular smooth muscle cells11 and valve interstitial cells) that transdifferentiate into osteoblast-like cells, and subsequently produce bone8,11,12. Indeed, the inorganic component of calcific lesions has an elemental composition similar to bone mineral13,14, and calcific lesions contain cells that express osteoblast-specific genes and form bone-specific proteins2,15. However, although end-stage calcific disease is marked by the accumulation of calcium phosphate mineral, only limited analyses have been carried out to characterize this material, and more importantly, very little is known about the processes that mediate its formation. Therefore, a more robust understanding of the early events that precede macroscopic calcific lesion formation and the material that forms as a result may lend insight into the aetiology of calcific cardiovascular disease and allow for the development of effective therapies to prevent or reverse it.

The application of materials science techniques to models of developing bone has provided remarkable insight into bone's composition and hierarchical architecture16 in addition to elucidating the physiochemical and cell-mediated processes that mediate its formation17,18. Nevertheless, similar analyses have not been applied to cardiovascular calcific lesions, despite their superficial similarity to bone. Therefore, by adopting a materials science approach, we analyzed the material comprising calcific lesions in cardiovascular tissues from more than 60 patients. Combining scanning electron microscopy with energy-dispersive X-ray spectroscopy (SEM-EDS), transmission electron microscopy (TEM) with EDS, and selected area electron diffraction (SAED) of regions sampled using a focused ion beam (FIB), we first investigated 32 AV from normal patients and patients at different stages of CAVD (Supplementary Table 1).

We first examined AV with SEM to visualize the topographical characteristics of the tissue. The surfaces of normal AV did not contain macroscopically observable calcific lesions and the tissue appeared smooth (Supplementary Fig. 1). Density-dependent colour SEM (DDC-SEM) micrographs further revealed relatively uniform surface densities (Fig. 1a/b), and elemental analysis by EDS established that the material was entirely organic (Supplementary Fig. 2). Conversely, micrographs of AV presenting macroscopic calcific lesions revealed

dense structures in three distinct forms – as spherical particles, fibers and compact material (Fig. 1c/d, e and f, respectively, and Supplementary Fig. 3 for a visual depiction of image processing techniques). EDS of all three dense structures revealed calcium and phosphorus, with small amounts of magnesium and carbon (Fig. 2), which is similar to the elemental composition of bone19.

Mineralized tissue identified histologically as lamellar bone20 and notable for the presence of bone-specific proteins and the expression of osteoblast-specific genes2,21, has been previously identified in AV calcific lesions15,20. However, while calcified fibers and compact material resemble microstructures in bone18,22, the calcium- and phosphorus-containing spherical particles which we observed here (ranging in size from 100 nm to 5 μm, mean 0.82 ± 0.67 μm, n=763), have not been previously described in bone or meticulously examined in AV.

That is, although spherical particles are apparent in EM images of atherosclerotic tissue examined by Mohr & Görz 23,24, among others13,14,25–28, they have never been extensively scrutinized. Matrix vesicles, which are known to play important roles in both bone29,30 and cardiovascular calcification29,31 share some superficial characteristics with the spherical particles, however, in accordance with others' observations23,24, when we conducted identical analyses on human bone, we failed to identify comparable structures (Supplementary Fig. 4a).

In AV, however, we observed spherical particles associated with 100% of the calcific lesions we examined (Fig. 3e/f) and between 83% and 100% of the non-calcified tissue areas in which calcific lesions were present in other areas of the AV (Fig. 3c/d). We also detected these particles in 80% of non-calcified AV tissue from patients that presented calcific lesions in another part of the cardiovascular system (Fig. 3b). Analysis of particle size showed a trend for increasing particle diameter with increasing disease severity (Supplementary Fig. 5). Surprisingly, we also identified the same particles on 46% of AV in which the cardiovascular system was apparently entirely free from calcific lesions (Fig. 3a). Conversely, both the calcium- and phosphorous-containing dense fibers and compact material were only observed within lesions (Fig. 3e/f) and never on adjacent soft tissue or other non-calcified areas. When we observed either structure, we invariably found them in association with the spherical particles (Fig. 1e/f). Taken together, these observations suggest that mineralized spherical particles are a fundamental feature of AV calcification. Their presence at all stages of CAVD, particularly in valves without macroscopic calcific lesions, further suggests that spherical particles are the first mineralized structure to form and may play a role in disease initiation and/or progression.

To test this hypothesis, we next analyzed tissue harvested from regions near compact calcification and compared it to that harvested from tissue on which only mineralized spherical particles were present. First, we immunogold labelled tissues for osteocalcin, a bone-specific protein and late marker of osteoblast differentiation. Like other investigators8, we observed osteocalcin labelling in tissue adjacent to compact calcification, but never in tissue in which only mineralized spherical particles were present. Next, we immunogold labelled tissue for early osteoblastic transcription factors, DNA binding proteins that

regulate expression of other genes involved in osteoblastic differentiation, including Runx2 and Sp7 (Osterix)32–34. Our analyses show that these markers were strongly expressed in cells near spherical particles, however, we failed to indentify these nuclear-localizing proteins in the dense, less cellular matrix near compact calcification (Supplementary Fig. 6). Taken together, these data suggest that the presence of spherical particles may precede the appearance of mature osteoblastic cells and dense mineralized matrix that contains osteocalcin. Furthermore, our observation of Runx2 and Sp7 expression in apparently healthy tissue but for the presence of particles similarly suggests that either the localization of spherical particles may contribute to early osteoblastic transdifferentiation of cardiovascular cells, or conversely, that the expression of early osteoblastic markers leads to the localization of the particles.

Despite the insights they provided into the structure of calcific lesions, our SEM analyses and associated immunogold labelling only afforded a superficial characterization of the dense material formed on diseased AV and lent little insight into its precise composition or nanoarchitecture. Therefore, we next aimed to examine the internal chemical make-up and underlying nano-level organization of calcific lesions. Standard ultramicrotome sectioning of calcified materials, however, can disrupt the distribution and organization of mineral, obfuscating composition and architecture35,36. Therefore, we devised a method to examine internal regions of AV lesions by delicately sectioning them with a FIB and then examined them by TEM with EDS and SAED.

When we examined the internal composition of AV calcific lesions, we found that they contained spherical particles abundant in calcium and phosphorus with small amounts of magnesium not only on leaflet surfaces, but also embedded within lesions (Fig. 4a/b/d). EDS mapping demonstrated that particles were either surrounded by an organic matrix or embedded within a calcium- and phosphorus-rich material (Fig. 4a/b and Supplementary Fig. 7 and 8). The internal structure of individual particles, however, was even more striking. Particles were composed of concentric, unfaceted mineral layers with varying electron density (Fig. 4c). Interestingly, SAED patterns were typical of highly crystalline hydroxyapatite (Fig. 4a/e and Supplementary Fig. 9) and spheres were significantly more crystalline than mineral in samples of native bone (as determined by the full-width at half maximum (FWHM) of the peaks corresponding to planes 211, 112 and 300 for bone and 211 for the spherical particles in the SAED spectrum: 6.7 ± 1.0 versus 2.9 ± 0.2 (A.U.; mean ± s.d.; n = 6; $p < 0.05$), Supplementary Fig. 4). In contrast, the dense calcium- and phosphorus-containing material that often surrounded spheres yielded diffraction patterns indicative of poorly crystalline apatite, which was less crystalline than either the spherical particles or apatite in mature bone (FWHM could not be measured as the peaks corresponding to planes 211, 112 and 300 were not distinct). Bone mineralization takes place within and along collagen fibers by nucleation and growth of calcium phosphate crystals, forming a poorly crystalline apatite composed of plate-like structures37,38. In contrast, the spherical particles we describe here were composed of highly crystalline hydroxyapatite, likely formed by the addition of apatite in concentric layers. These observations suggest that mineralized spheres are not formed through a previously described biomineralization process, but rather by a different mechanism, one that varies from the process that forms either bone or the dense compact material that comprises lesions.

The ubiquitous presence of spherical particles in our AV samples next prompted us to question whether other calcification in the cardiovascular system exhibited similar material characteristics. Other calcific cardiovascular diseases, such as rheumatic fever and arteriosclerosis, however, are often studied independently, as their clinical manifestations and the demographics they affect are quite distinct8,15,39. Therefore, we followed our analyses of AV with an identical characterization of 17 mitral valves, 14 coronary arteries, and 22 aortas from rheumatic fever, CAVD and arteriosclerosis patients (for patient information and analyses of calcified structures by disease severity, see Supplementary Table 2 and Supplementary Fig. 10, respectively). Our nano-analytical electron microscopy analyses demonstrated that the calcified material comprising lesions from all tissues had the same architecture (Fig. 5a-f and Supplementary Fig. 11), composition and crystallinity (Fig. 5g and Supplementary Fig. 12) as that observed in AV. As before, TEM images of FIB sectioned lesions were notable for highly crystalline, calcium- and phosphorus-rich spherical particles that failed to intimately associate with collagen fibrils as mineral crystals do in bone (Fig. 5g). Similarly to our previous analyses, again we detected highly crystalline hydroxyapatite spherical particles in tissues that did not present macroscopic calcification, which suggests that spherical particles are not only the first mineralized structure formed in cardiovascular tissues, but also that the formation of calcific lesions among apparently disparate diseases may follow a common process.

Collectively, these data form the basis for a new paradigm in cardiovascular calcification. Nevertheless, it remains uncertain what role the spherical particles may or may not play in mediating lesion formation. Huipin *et al.*40 and others have demonstrated that both subcutaneous41,42 and intramuscular40,43,44 implantation of calcium phosphates drives bone formation *via* the recruitment and/or transdifferentiation of local or circulating cells that subsequently adopt a mineralizing phenotype45–47. If a similar mechanism could drive the formation of calcific lesions, this might suggest that the localization of mineralized spherical particles could initiate a similar process that would then drive the formation of compact calcification in a cell-mediated process. Although the mechanism by which the presence of calcium phosphate promotes the formation of bone-like material remains unclear45,47, there is evidence that valve interstitial cells may participate in such a process and could be responsible for lesion formation21,48. Furthermore, recent insights into the role of substrate stiffness in stem cell differentiation may likewise explain cell transdifferentiation and/or recruitment49, as stiffer matrices (which mineralized spherical particles would presumably provide) have been shown to drive mesenchymal stem cells towards an osteoblast phenotype50. In short, while recruitment and/or cell transdifferentiation may promote the formation of calcific lesions, this does not preclude the likelihood that initial calcification events were not mediated by this process and opens the possibility that spherical mineralized particles play a role.

Furthermore, our observations here of an identical material in tissues from patients with a range of calcific cardiovascular diseases, even when macroscopic calcific lesions were absent, may suggest that the formation of calcific lesions follows a common process. These observations open the possibility of a unified model for calcification in the cardiovascular system that reconciles previous reports of osteoblastic cells and bone-like tissue with our evidence that the material comprising lesions is distinct from bone mineral. It also presents

the opportunity to consider alternative therapies to prevent or reverse calcific disease. Our materials science perspective provides unique guidance in this regard. A direct consequence of our ability to analyse FIB-sectioned particles by SAED would suggest that targeting the spherical particles themselves for dissolution, for example, would be unsuccessful as poorly crystalline, healthy bone mineral would preferentially be affected over the highly crystalline spherical particles. Therapies that rather aim to either prevent their formation or adherence to cardiovascular tissue may be more successful. Moreover, similar analyses of tissue from patients with calcific cardiovascular disease who have undergone various interventions may prompt a new understanding of why some therapies may be more effective than others. Future studies in experimental animal models may likewise benefit from the application of these methods as an additional 'phenotyping' to determine if they truly emulate the human disease. In short, our materials science insights may have important implications for understanding calcific cardiovascular disease and developing therapies to treat or prevent it, and highlights the importance of an interdisciplinary approach in medicine.

Methods

Sample preparation

32 human aortic valves (AV) were provided by Old Brompton Hospital-London or by Oxford Heart Valve Bank at John Radcliffe Hospital – Oxford, and obtained from either patients undergoing AV replacement surgery or were AV that had been rejected for use as homografts. Mitral valve, aorta and coronary artery samples were provided by Old Brompton Hospital – London, the Heart Valve Bank at the John Radcliffe Hospital – Oxford, and Aswan Hospital - Chain of Hope charity mission to Africa (n = 17 mitral valves, n = 14 coronary arteries and n = 22 aortas). Human femoral head bone samples from patients undergoing elective total hip arthroplasty procedures were kindly provided by Mr. Alister Hart from Charing Cross Hospital – London. All samples were collected under approved ethical guidelines with informed consent that allowed us to anonymously analyse the tissues. These ethics precluded further access to patient medical history and pharmacological therpies and only provided the data given in Supplementary Tables 1 and 2.

Bone and cardiovascular tissue samples were fixed in a 4% (w/v) formaldehyde (Sigma, BioReagent, ≥36.0%) solution in phosphate buffered saline (PBS; Sigma) at room temperature for at least 1 day immediately upon receipt. Samples were then dehydrated through a graded ethanol (Sigma, ACS reagent 99.5%) series (20, 30, 40, 50 70, 80, 90, 100 and 100% (v/v)) for one hour in each solution and air dried. Several regions of each dried sample were systemically dissected and categorized by disease severity as detailed in the legend for Figure 3. Samples from the surface and the interior of each sample were extracted using common dissection tools. Following dissection, samples were prepared for SEM/FIB.

Scanning electron microscopy (SEM) analyses and focused ion beam (FIB) preparation

Samples were secured to an aluminium sample holder with carbon tape, and silver paint was applied to the area immediately surrounding each sample, which was then coated with 5 nm carbon (Quorum Technologies Turbo-Pumped Thermal Evaporators model K975X) and 5 nm chromium in a sputter coater (Quorum Technologies Sputter Coater model K575X).

Scanning electron microscopy (SEM) and energy-dispersive X-ray spectroscopy (EDS) analyses

Following the coating procedure, samples were imaged by SEM (Gemini 1525 FEGSEM), operated at 10kV. The instrument was equipped with both an inlens detector which recorded secondary electrons, and a backscatter electron detector. The density-dependent colour SEM images were obtained by imaging a region in inlens mode and subsequently imaging the same region in backscatter mode. Using ImageJ software, both images where stacked and the inlens image was assigned to the green channel whereas the backscatter image was assigned to the red channel (for more details, see Supplementary Fig 3). EDS were obtained in the regions of interest using the point and shoot mode, which focuses the beam on the selected region and provides a spatial resolution of 3μm.

Focused ion beam (FIB)

Following SEM analysis, samples were transferred to a focused ion beam (FEI FIB200-SIMS or a SEM/Focused Ion Beam Helios NanoLa 50 series Dual Beam). A region 20 x 2 μm was coated with a 2 μm thick platinum layer (93pA at 30kV) to protect the sample surface from the gallium beam during the milling and polishing process. Two trenches of 20 x 10 x 10 μm (length x height x depth) were made using currents between 2.8 nA and 21 nA parallel to the platinum protective layer creating a section with dimensions of 20 x 2 x 10 μm. The section was thinned with the beam until it was 1 μm thick using a current between 93 pA and 2.8 nA. After the rough thinning, the base of the section was cut using a current of 2.8 nA. With a micromanipulator needle, the resulting section was then attached to a FIB lift-out grid using platinum. The section was then thinned again, until it was approximately 100 nm thick using beam currents between 28 pA and 2.8 nA. Finally, to clean the surface and remove possible artefacts introduced by the milling, the resulting surface was polished with a gallium beam operated at 2 kV.

Transmission electron microscopy (TEM), energy-dispersive X-ray spectroscopy (EDS) and selected area electron diffraction (SAED) analyses

Samples extracted and prepared by FIB were imaged in the TEM at 120kV on a JEOL 2000FX TEM or JEOL 2010 TEM. Elemental maps were obtained by EDS in the TEM operating at 200kV (Oxford Instruments INCA EDS 80mm X-Max detector system with SemiSTEM capability), which provided a spatial resolution of 50 nm. SAED were obtained in the TEM operating at 120kV.

FWHM

The full-width at half maximum (FWHM) of the peak corresponding to planes 211, 112 and 300 for bone and 211 for the spherical particles in the SAED spectra was determined using the “Plot Profile” function in ImageJ. The FWHM, which is reported as arbitrary units, was measured by quantifying pixels using Origin 6.0. Differences between the FWHM of spectra obtained from human bone and spherical particles from AV samples were determined using a Mann-Whitney U test. Differences were considered statistically significant when $p < 0.05$.

Immunogold labelling

MC3T3-E1 murine pre-osteoblastic cells were obtained from the American Type Culture Collection and routinely cultured in Alpha Minimum Essential medium supplemented with 15% (v/v) fetal bovine serum (both from Invitrogen). Cells were plated at 30,000 cell cm^{-1} and cultured for either 24 hours (Runx2 and SP7 staining) or 14 days (osteoclacin staining) in osteogenic medium, which contained growth medium supplemented with 50 μg/mL ascorbic acid and 10 mM β-glycerosphosphate (both from Sigma). Aortic valve samples and cells on tissue culture plastic were fixed in a 4% (w/v) formaldehyde (Sigma, BioReagent, ≥36.0%) solution in phosphate buffered saline (PBS; Sigma) at room temperature for at least 1 day immediately upon receipt (tissue) or at least 15 min (cells). Cells were scraped from the culture surface with a rubber policeman and pelleted. Samples were then dehydrated through a graded ethanol (Sigma, ACS reagent 99.5%) series (20, 30, 40, 50 70, 80, 90, 100, 100, 100% (v/v)) for one hour (tissue) or 15 min (cells) in each solution. After dehydration, samples were infiltrated with Lowicryl Resin (EMS sciences HM20) diluted in ethanol at 3:1, 2:1, and 1:1 for 3 hours each, and then over night at 1:2. The solution was then replaced with pure resin, which was changed twice in the first 12 hours and then allowed to infiltrate again overnight. Finally, the resin was changed again and then curetted with UV light (365 nm wavelength) at 4°C for 4 days.

Curetted resin blocks were sectioned at 100 nm in an ultramicrotome (Leica) and immediately placed on carbon-coated copper grids. The grids were then floated in a 10 μl drop of (2% v/v in water) glycerine solution for 5 minutes, then in blocking agent (4% (w/v) bovine serum albumin (BSA) + 2% (w/v) cold fish skin gelatine in PBS for all samples except collagen, for which the blocking agent consisted of 4% BSA alone) for 15 minutes. Grids were then washed 5 times on 10 μL drops of the blocking agent for 2 minutes each and floated for 1 hour in a 10 μl drop containing the primary antibody diluted in the blocking agent (Abcam Anti-Osteocalcin antibody, mouse monoclonal, concentration of 1:200; Abcam Anti-RUNX2 antibody, rabbit polyclonal, concentration 1:100; Abcam Anti-SP7/Osterix antibody, ChIP grade, rabbit polyclonal, concentration 1:300; and Abcam Anti-Collagen I antibody, rabbit polyclonal concentration 1:50). Grids were then washed 5 times on drops of the blocking agent for 2 minutes each and then floated in 10 μL drops of Immunogold solution (Aurion10 nm - Anti-Mouse and Aurion 6 nm - Anti-Rabbit concentration for both of 1:30) for 1 hour. Grids were then washed 5 times with the blocking agent for 2 minutes each, twice with deionized water for 5 minutes each, and then floated for 5 minutes in a solution of 2% (w/v) glutaraldehyde in water, before they were again washed 5 times in deionized water for 2 minutes each and finally air dried. The grids were imaged in the TEM at 80kV (JEOL 2000FX TEM).

Supplementary Material

Refer to Web version on PubMed Central for supplementary material.

Acknowledgements

S.B. was supported by the Rosetrees Trust and the Junior Research Fellowship scheme at Imperial College London. E.G. was supported by a fellowship from the Wellcome Trust. K.L.C. was supported by a fellowship from the

British Heart Foundation. M.M.S. gratefully acknowledges funding from the Rosetrees Trust and from the ERC grant Naturale.

References

1. Butler D. UN targets top killers. Nature. 2011:260–261.
2. Rajamannan NM, et al. Human aortic valve calcification is associated with an osteoblast phenotype. Circulation. 2003; 107:2181–2184. [PubMed: 12719282]
3. Lindroos M, Kupari M, Heikkila J, Tilvis R. Prevalence of aortic valve abnormalities in the elderly: an echocardiographic study of a random population sample. J Am Coll Cardiol. 1993; 21:1220–1225. [PubMed: 8459080]
4. Nkomo VT, et al. Burden of valvular heart diseases: a population-based study. Lancet. 2006; 368:1005–1011. [PubMed: 16980116]
5. Roger VL, et al. Heart Disease and Stroke Statistics—2011 Update. Circulation. 2011; 123:e18–e209. [PubMed: 21160056]
6. Iung B, Vahanian A. Epidemiology of valvular heart disease in the adult. Nat Rev Cardiol. 2011; 8:162–172. [PubMed: 21263455]
7. Sekikawa A, et al. Aortic stiffness and calcification in men in a population-based international study. Atherosclerosis. 2012; 222:473–477. [PubMed: 22537531]
8. Sage AP, Tintut Y, Demer LL. Regulatory mechanisms in vascular calcification. Nat Rev Cardiol. 2010; 7:528–536. [PubMed: 20664518]
9. Langanay T, et al. Aortic valve replacement in the elderly: The real life. Ann Thorac Surg. 2012; 93:70–78. [PubMed: 21982149]
10. Thomas M, et al. Thirty-day results of the sapien aortic bioprosthesis european outcome (source) registry. Circulation. 2010; 122:62–69. [PubMed: 20566953]
11. Duer MJ, et al. Mineral surface in calcified plaque is like that of bone further evidence for regulated mineralization. Arterioscler Thromb Vasc Biol. 2008; 28:2030–U2208. [PubMed: 18703777]
12. Mody N, Tintut Y, Radcliff K, Demer L. Vascular calcification and its relation to bone calcification: Possible underlying mechanisms. J Nucl Cardiol. 2003; 10:177–183. [PubMed: 12673183]
13. Delogne C, Lawford PV, Habesch SM, Carolan VA. Characterization of the calcification of cardiac valve bioprostheses by environmental scanning electron microscopy and vibrational spectroscopy. J Microsc. 2007; 228:62–77. [PubMed: 17910699]
14. Weska RF, et al. Natural And Prosthetic Heart Valve Calcification: Morphology And Chemical Composition Characterization. Artif Organs. 2010; 34:311–318. [PubMed: 20420613]
15. Demer LL, Tintut Y. Vascular calcification: Pathobiology of a multifaceted disease. Circulation. 2008; 117:2938–2948. [PubMed: 18519861]
16. Fratzl P, Weinkamer R. Nature's hierarchical materials. Prog Mater Sci. 2007; 52:1263–1334.
17. Gentleman E, et al. Comparative materials differences revealed in engineered bone as a function of cell-specific differentiation. Nat Mater. 2009; 8:763–770. [PubMed: 19633661]
18. Mahamid J, et al. Mapping amorphous calcium phosphate transformation into crystalline mineral from the cell to the bone in zebrafish fin rays. P Natl Acad Sci Usa. 2010; 107
19. Biltz RM, Pellegri Ed. Chemical anatomy of bone. I.A. Comparative study of bone composition in 16 vertebrates. J Bone Joint Surg-Am Vol. 1969; A 51:456.
20. Mohler ER III, et al. Bone formation and inflammation in cardiac valves. Circulation. 2001; 103:1522–1528. [PubMed: 11257079]
21. Rajamannan NM, et al. Calcific aortic valve disease: Not simply a degenerative process. Circulation. 2011; 124
22. Su X, Sun K, Cui FZ, Landis WJ. Organization of apatite crystals in human woven bone. Bone. 2003; 32:150–162. [PubMed: 12633787]
23. Mohr W, Görz E. Verkalkungen der temporalarterien - ihre morphogenese im vergleich zur physiologischen osteogenese. Z Kardiol. 2003; 92:60–72. [PubMed: 12545303]

Europe PMC Funders Author Manuscripts

24. Mohr W, Gorz E. Does calcification of arteriosclerotic vessels imitate osteogenesis? Pathomorphological study of arteriosclerotic plaques. Z Kardiol. 2002; 91:212–232. [PubMed: 12001537]
25. Kockx MM, Muhring J, Bortier H, DeMeyer GRY, Jacob W. Biotin- or digoxigenin-conjugated nucleotides bind to matrix vesicles in atherosclerotic plaques. Am J Pathol. 1996; 148:1771–1777. [PubMed: 8669464]
26. Johnston KW, et al. Determining the quantity and character of carotid artery embolic debris by electron microscopy and energy dispersive spectroscopy - Discussion. J Vasc Surg. 2007; 45:724–725.
27. Miller VM, et al. Evidence of nanobacterial-like structures in calcified human arteries and cardiac valves. Am J Physiol Heart Circ Physiol. 2004; 287:H1115–1124. [PubMed: 15142839]
28. Koutsopoulos S, Kontogeorgou A, Dalas E, Petroheilos J. Calcification of porcine and human cardiac valves: testing of various inhibitors for antimineralization. J Mater Sci-Mater M. 1998; 9:421–424. [PubMed: 15348871]
29. Anderson H. Matrix vesicles and calcification. Current Rheumatology Reports. 2003; 5:222–226. [PubMed: 12744815]
30. Boonrungsiman S, et al. The role of intracellular calcium phosphate in osteoblast-mediated bone apatite formation. P Natl Acad Sci Usa. 2012; 109:14170–14175.
31. Tanimura A, McGregor DH, Anderson HC. Matrix vesicles in artherosclerotic calcification. Proc Soc Exp Biol Med. 1983; 172:173–177. [PubMed: 6828462]
32. Komori T, et al. Targeted disruption of cbfa1 results in a complete lack of bone formation owing to maturational arrest of osteoblasts. Cell. 1997; 89:755–764. [PubMed: 9182763]
33. Satokata I, et al. Msx2 deficiency in mice causes pleiotropic defects in bone growth and ectodermal organ formation. Nature Genet. 2000; 24:391–395. [PubMed: 10742104]
34. Nakashima K, et al. The novel zinc finger-containing transcription factor osterix is required for osteoblast differentiation and bone formation. Cell. 2002; 108:17–29. [PubMed: 11792318]
35. Jantou V, Turmaine M, West GD, Horton MA, McComb DW. Focused ion beam milling and ultramicrotomy of mineralised ivory dentine for analytical transmission electron microscopy. Micron. 2009; 40:495–501. [PubMed: 19157888]
36. McNally EA, Schwarcz HP, Botton GA, Arsenault AL. A model for the ultrastructure of bone based on electron microscopy of ion-milled sections. PLoS One. 2012; 7:e29258. [PubMed: 22272230]
37. Landis WJ, Hodgens KJ, Arena J, Song MJ, McEwen BF. Structural relations between collagen and mineral in bone as determined by high voltage electron microscopic tomography. Microsc Res Tech. 1996; 33:192–202. [PubMed: 8845518]
38. Nudelman F, et al. The role of collagen in bone apatite formation in the presence of hydroxyapatite nucleation inhibitors. Nat Mater. 2010; 9:1004–1009. [PubMed: 20972429]
39. New SEP, Aikawa E. Cardiovascular calcification: An inflammatory disease. Circulation Journal. 2011; 75:1305–1313. [PubMed: 21566338]
40. Yuan H, et al. Osteoinductive ceramics as a synthetic alternative to autologous bone grafting. P Natl Acad Sci Usa. 2010; 107:13614–13619.
41. Yamasaki H, Sakai H. Osteogenic response to porous hydroxyapatite ceramics under the skin of dogs. Biomaterials. 1992; 13:308–312. [PubMed: 1318086]
42. Yang ZJ, et al. Osteogenesis in extraskeletally implanted porous calcium phosphate ceramics: Variability among different kinds of animals. Biomaterials. 1996; 17:2131–2137. [PubMed: 8922598]
43. Kurashina K, Kurita H, Wu Q, Ohtsuka A, Kobayashi H. Ectopic osteogenesis with biphasic ceramics of hydroxyapatite and tricalcium phosphate in rabbits. Biomaterials. 2002; 23:407–412. [PubMed: 11761160]
44. Le Nihouannen D, et al. Ectopic bone formation by microporous calcium phosphate ceramic particles in sheep muscles. Bone. 2005; 36:1086–1093. [PubMed: 15869915]
45. Ducheyne P, Qiu Q. Bioactive ceramics: the effect of surface reactivity on bone formation and bone cell function. Biomaterials. 1999; 20:2287–2303. [PubMed: 10614935]

46. LeGeros RZ. Properties of osteoconductive biomaterials: Calcium phosphates. Clin Orthop Rel Res. 2002:81–98.
47. LeGeros RZ. Calcium phosphate-based osteoinductive materials. Chem Rev. 2008; 108:4742–4753. [PubMed: 19006399]
48. Miller JD, Weiss RM, Heistad DD. Calcific aortic valve stenosis: methods, models, and mechanisms. Circ Res. 2011; 108:1392–1412. [PubMed: 21617136]
49. Chen JH, Simmons CA. Cell-matrix interactions in the pathobiology of calcific aortic valve disease critical roles for matricellular, matricrine, and matrix mechanics cues. Circ Res. 2011; 108:1510–1524. [PubMed: 21659654]
50. Engler AJ, Sen S, Sweeney HL, Discher DE. Matrix elasticity directs stem cell lineage specification. Cell. 2006; 126:677–689. [PubMed: 16923388]

Europe PMC Funders Author Manuscripts

Europe PMC Funders Author Manuscripts

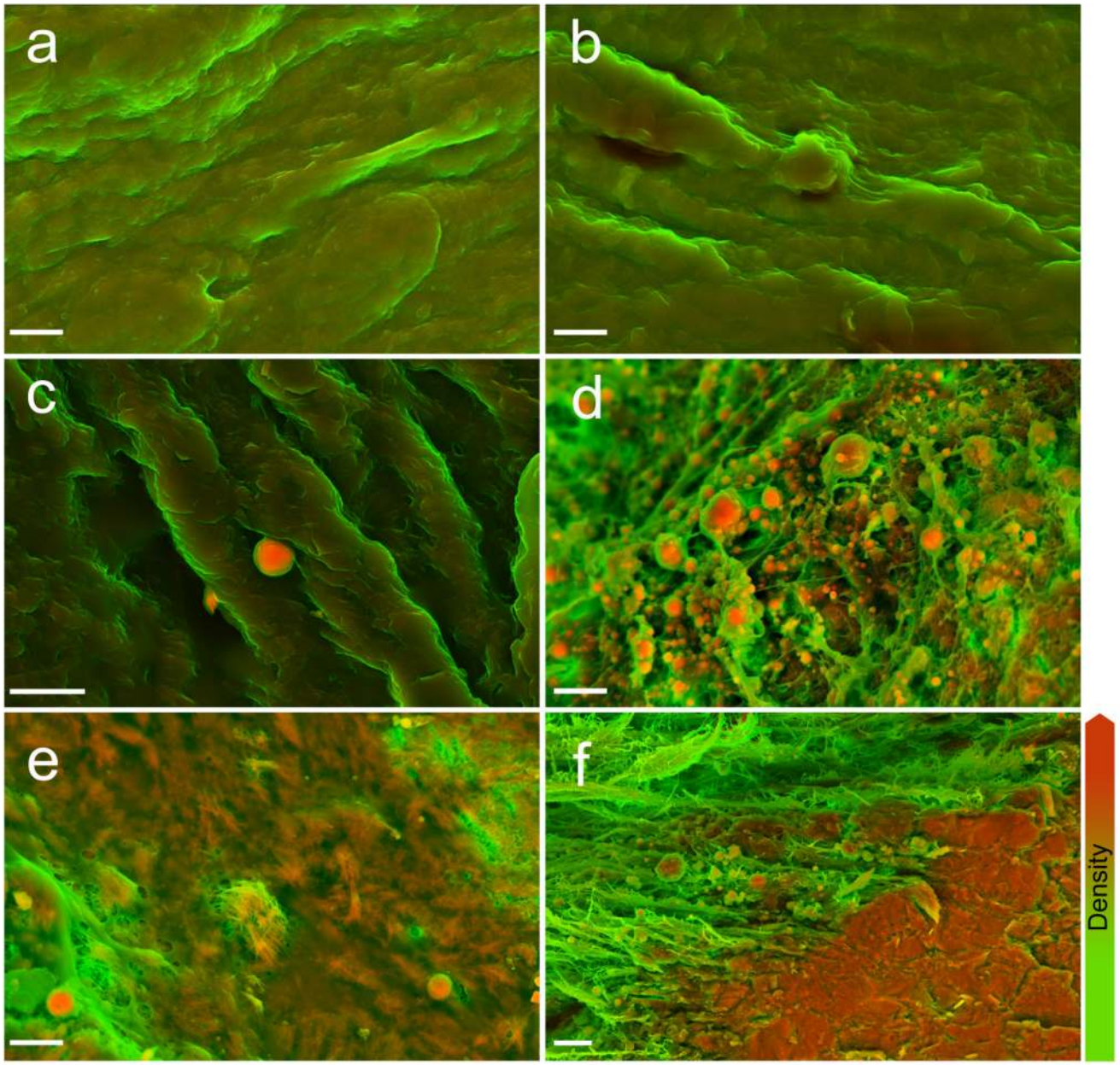

Figure 1. Density-dependent color scanning electron micrographs of human aortic valve (AV) tissue.

Micrographs were coloured in post-processing by combing images acquired by secondary and backscatter electron detectors (details and original images are in Supplementary Fig. 3). The orange colour identifies denser material, while structures that appear green are less dense. **a, b** Surface of AV rejected for transplant because of physical damage. Samples lacked macroscopic calcific lesions and were judged not to be atheromic. **c** Surface of AV free from macroscopically observable calcific lesions, but presenting dense spherical particles. **d** Calcific lesion on AV with notable dense spherical particles. **e** Calcific lesion on

AV, presenting dense spherical particles and fibers. **f** Calcific lesion on AV, presenting dense spherical particles and compact material. Scale bar = 3 μm.

Europe PMC Funders Author Manuscripts

Europe PMC Funders Author Manuscripts

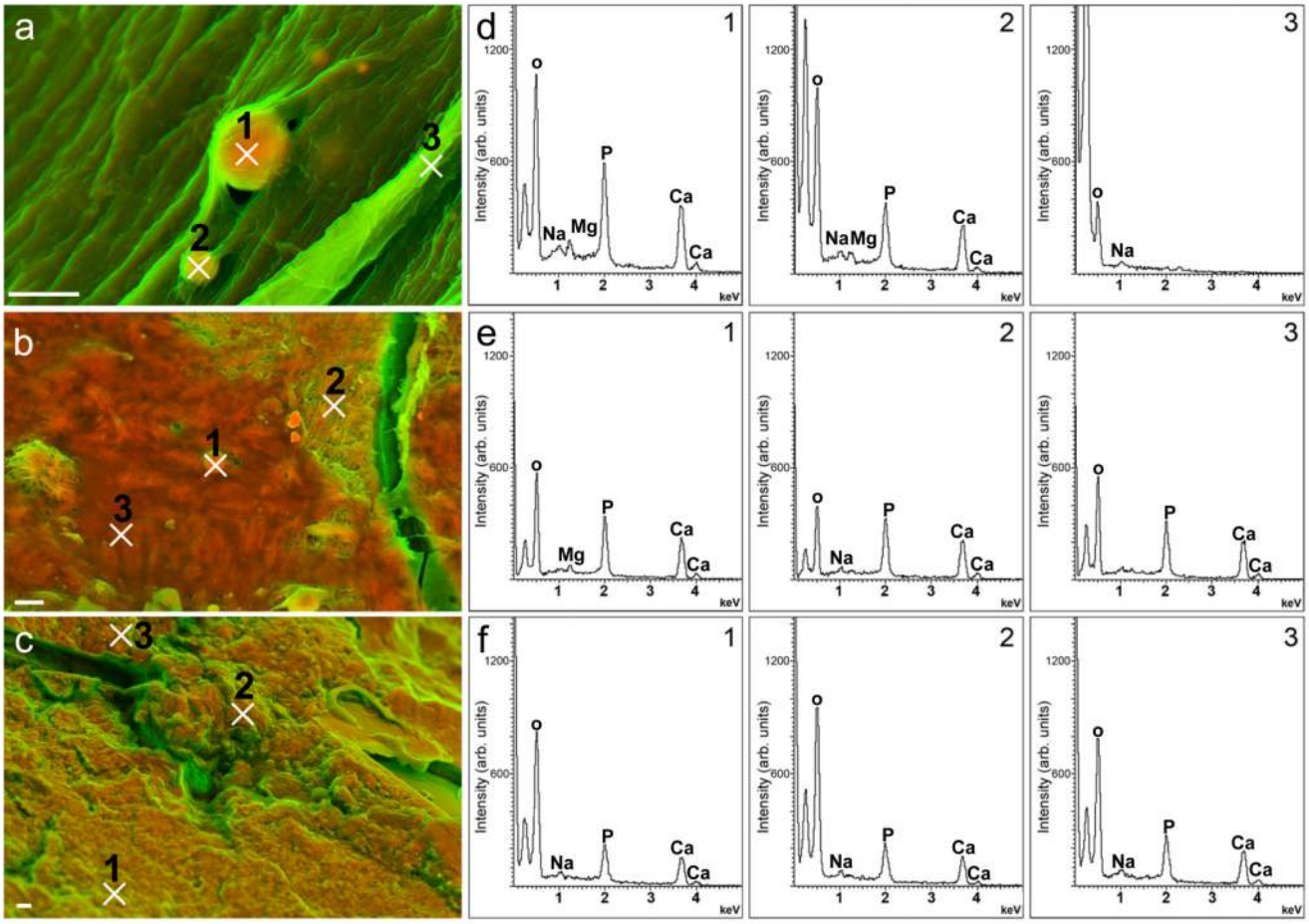

Figure 2. Elemental analyses of dense structures identified on aortic valves (AV).

Density-dependent colour scanning electron micrographs of AV presenting **(a)** dense spherical particles, **(b)** dense fibers and (**c**) compact material. **d, e** and **f** depict corresponding energy-dispersive X-ray spectra collected at the numbered sites indicated on micrographs **a, b** and **c**, respectively. Scale bar: 2 = μm.

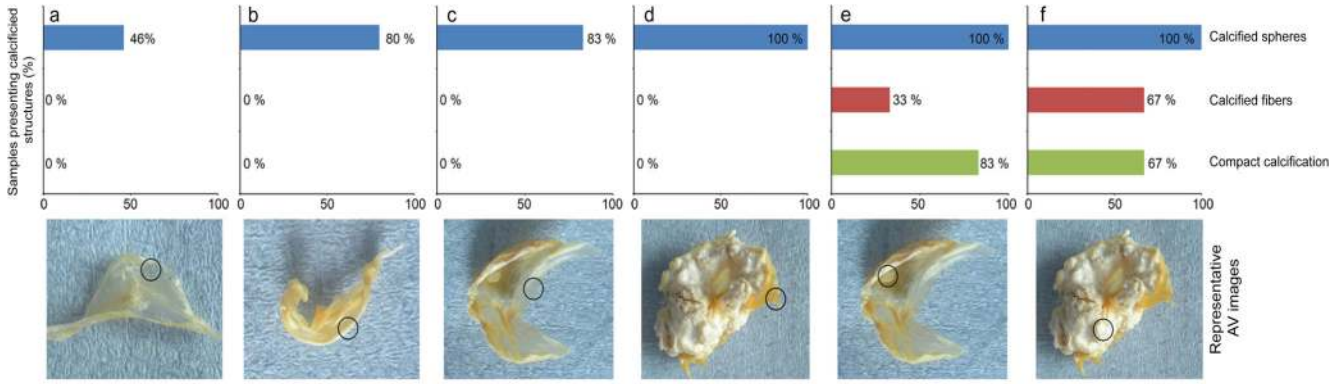

Figure 3. Histogram describing the prevalence of dense calcium- and phosphorus-containing structures on the surface of aortic valves (AV).

Representative images of AV are categorized by presence and extensiveness of calcific lesions. Sampled regions indicated in circles. Category **a** is comprised of AV that did not present any macroscopically observable calcific lesions on AV or in surrounding tissue (aorta and coronary arteries). **b** represents AV without macroscopically observable calcification on AV, but with macroscopically observable calcific lesions on surrounding tissues. **c** includes analyses carried out on non-calcified areas of AV which presented calcific lesions in other areas of the AV. **d** includes analyses carried out on non-calcified areas of AV which were heavily calcified in other areas. **e** identifies structures on macroscopically observable calcific lesions. f includes analyses carried out on calcific lesions from heavily calcified AV. Approximately 350 images were obtained from each of the 55 regions examined in AV from 32 patients.

Europe PMC Funders Author Manuscripts

Europe PMC Funders Author Manuscripts

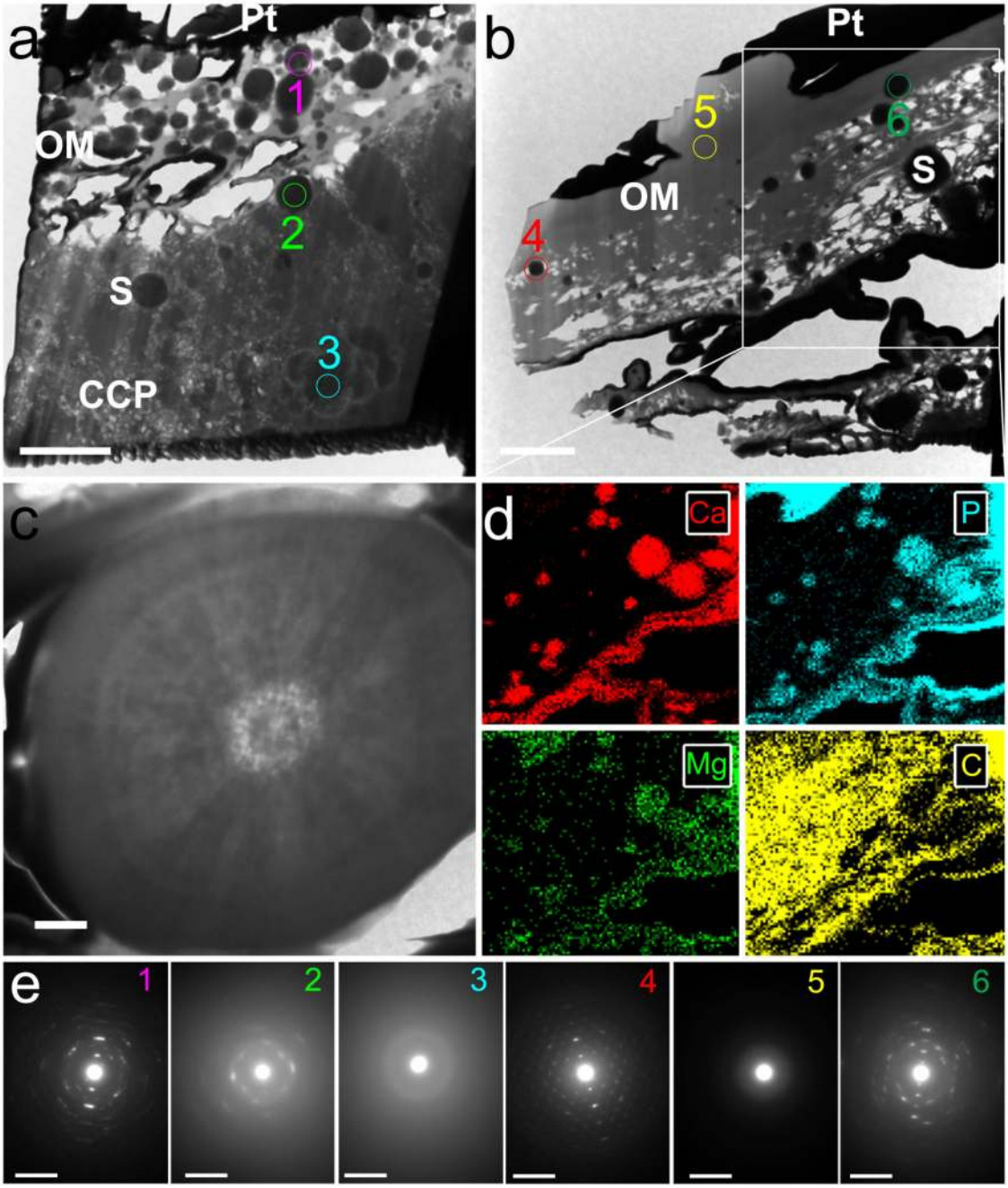

Figure 4. Transmission electron microscopy (TEM) images, energy-dispersive X-ray spectroscopy (EDS) mapping, and selected area electron diffraction (SAED) analyses of aortic valve (AV) tissues sectioned with a focussed ion beam (FIB).

a/b TEM images show spherical particles (S) trapped in compact calcium phosphate (CCP) and organic matrices (OM). AV surfaces are coated in a dense layer of platinum (Pt) utilized in sample preparation for FIB. Scale bar = 2 μm. **c** High-resolution TEM of calcium- and phosphorus-containing spherical particle on the surface of a calcific lesion. Scale bar = 0.2 μm. **d** Elemental mapping of calcium (Ca), phosphorus (P), magnesium (Mg) and carbon (C) in the region inside the highlighted area in **b** (original images and elemental maps of

gallium, the ion source utilized by the FIB, and platinum are included in Supplementary Figs. 5/6). **e** SAED obtained from each of the sections inside the numbered circles in **a** and **b.** Scale bar = 0.05 nm-1. Note that spherical particles produce diffraction patterns typical of highly crystalline material, while the surrounding compact material yielded diffraction patterns typical of a poorly crystalline material.

Europe PMC Funders Author Manuscripts

Europe PMC Funders Author Manuscripts

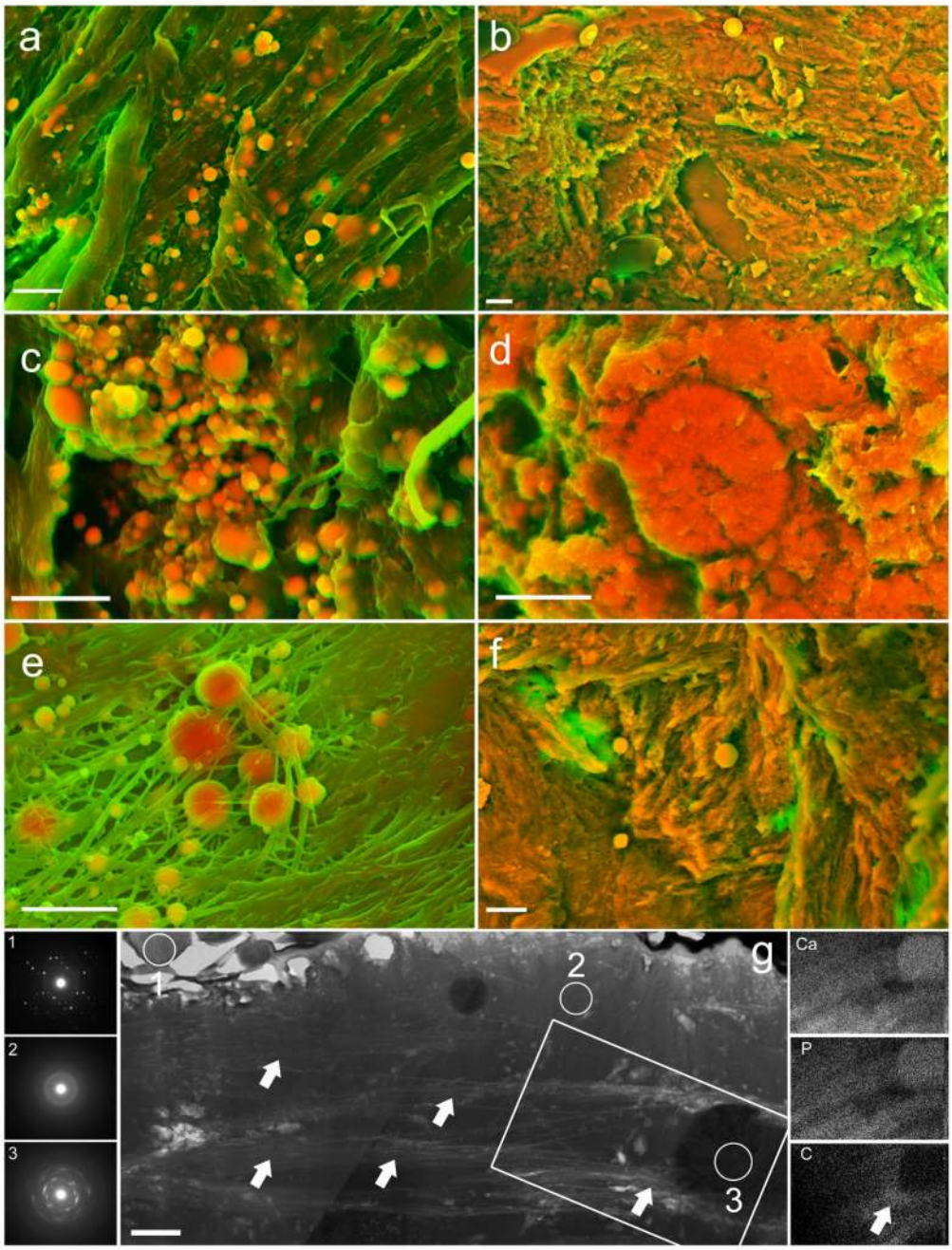

Figure 5. Density-dependent colour scanning electron micrographs of mitral valve, aorta and coronary artery, and transmission electron microscopy (TEM), selected area electron diffraction (SAED) and energy dispersion X-ray spectroscopy (EDS) mapping of calcific lesions on coronary artery tissue sectioned using a focussed ion beam (FIB).

a Mitral valve tissue with notable dense spheres. **b** Calcific lesion on mitral valve tissue presenting dense spherical particles and compact material. **c** Aortic tissue with notable dense spherical particles. **d** Calcific lesion on aortic tissue presenting dense spherical particles and compact material. **e** Coronary artery tissue with dense spherical particles. **f** Calcific lesion on coronary artery presenting dense spherical particles and compact material. Further examples

of dense structures and dense fibers are provided in Supplementary Fig. 7. Scale bar = 3 μm. **g** TEM of a calcific lesion on coronary artery tissue shown with SAED images of the numbered regions (left-hand column) and elemental mapping by EDS (right-hand column) of areas highlighted in the central image. Arrows point to collagen fibers, which are notably not intimately associated with the mineralized spherical particles. Scale bar = 2 μm.

Europe PMC Funders Author Manuscripts